

Classical Molecular Dynamics Simulation of the Photoinduced Electron Transfer Dynamics of Plastocyanin

Lowell W. Ungar, Norbert F. Scherer, and Gregory A. Voth

Department of Chemistry, University of Pennsylvania, Philadelphia, Pennsylvania 19104-6323 USA

ABSTRACT Classical molecular dynamics simulations are used to investigate the nuclear motions associated with photoinduced electron transfer in plastocyanin. The blue copper protein is modeled using a molecular mechanics potential; potential parameters for the copper-protein interactions are determined using an x-ray crystallographic structure and absorption and resonance Raman spectra. Molecular dynamics simulations yield a variety of information about the ground (oxidized) and optically excited (charge-transfer) states: 1) The probability distribution of the potential difference between the states, which is used to determine the coordinate and energy displacements, places the states well within the Marcus inverted region. 2) The two-time autocorrelation function of the difference potential in the ground state and the average of the difference potential after instantaneous excitation to the excited state are very similar (confirming linear response in this system); their decay indicates that vibrational relaxation occurs in about 1 ps in both states. 3) The spectral densities of various internal coordinates begin to identify the vibrations that affect the optical transition; the spectral density of the difference potential correlation function should also prove useful in quantum simulations of the back electron transfer. 4) Correlation functions of the protein atomic motions with the difference potential show that the nuclear motions are correlated over a distance of more than 20 Å, especially along proposed electron transport paths.

INTRODUCTION

Electron transfer is one of the most common functions of proteins (Moser et al., 1992, 1995). Although it is inherently an electronic process, i.e., a transition between two electronic states, electron transfer is facilitated by nuclear motion in the protein and in the surrounding solvent. For intermolecular electron transfer such motions can bring the molecules within an appropriate distance for reaction. For inter- and intramolecular processes, vibrational fluctuations serve to bring the energies of the electronic states sufficiently close that transfer can occur under the Franck-Condon conditions of no change in nuclear positions or momentum (Marcus, 1956; Marcus and Sutin, 1985; Levich and Dogonadze, 1959; Jortner, 1976). Further vibrational motion is induced by the electronic transition, as the nuclei react to the new potential, causing vibrational relaxation and solvation.

The specific vibrational motions associated with activated or long-range electron transfer are difficult to study by either simulation or experiment because, although a single electronic transition is fast, the frequency of electron transfer events is typically slow on a vibrational time scale (μs^{-1} or ms^{-1} versus fs^{-1}) (Moser et al., 1992). In simulations such infrequent events can be studied using umbrella sampling (Allen and Tildesley, 1987) and similar methods if the transition state is known, but it would be easier to study the electron transfer dynamics in real time if the process were externally induced. This is one reason for examining a

photoinduced electron transfer process using either simulations or ultrafast optical spectroscopy (Reid et al., 1995; Arnett et al., 1995). In addition, the free energy fluctuations associated with vibrational fluctuations in the photoexcited electronic state often can be simply related to those of other states (Tachiya, 1993).

Type I blue copper proteins (Sykes, 1991a,b; Solomon et al., 1992) are excellent subjects for this kind of study. Ranging from single copper-center proteins such as plastocyanin, azurin, and stellacyanin to large multisite proteins such as ceruloplasmin, blue copper proteins transport electrons and serve as redox reagents in many plants and bacteria. Plastocyanin (Redinbo et al., 1994), for example, in its oxidized state accepts an electron from cytochrome *f* in photosystem II and transfers it to a chlorophyll in photosystem I. But blue copper proteins, as their name implies, also have a strong optical transition around 600 nm, which has been identified formally as a ligand-to-copper electron transfer (Solomon et al., 1980; Gewirth and Solomon, 1988). Thus one can study the vibrations associated with both the optical electronic transition and the subsequent electron transfer from the excited state back to the ground state. The back electron transfer is perhaps more similar to the naturally occurring process.

In this paper the vibrations associated with photoinduced electron transfer in plastocyanin are investigated using classical molecular dynamics (MD); and the protein is modeled by a molecular mechanics potential. The parameters for the normal protein atoms are from CHARMM (Brooks et al., 1983); new parameters for the copper-protein interaction were chosen for consistency with the existing parameter set and with experimental data. The optically excited state is modeled by a small displacement from the ground state. Because the focus is mostly on the copper center, the protein

Received for publication 28 May 1996 and in final form 15 October 1996.

Address reprint requests to Dr. Gregory A. Voth, Department of Chemistry, University of Utah, Salt Lake City, UT 84112. Tel.: 801-581-7272; E-mail: voth@chemistry.chem.utah.edu.

© 1997 by the Biophysical Society

0006-3495/97/01/05/13 \$2.00

is solvated only by the 109 water molecules identified in the crystallographic structure, and the simulation cell does not include periodic boundary conditions or replicas.

Although the classical MD simulations reported here cannot directly simulate the electronic transition between the states, they can illuminate the vibrational dynamics associated with the electron transfer. The simulations examine both the nuclear fluctuations in thermal equilibrium in the ground electronic state and the nuclear motion after instantaneous excitation of the thermal distribution to the excited state. In both cases analysis focuses on the potential difference between the two states (i.e., the coordinate-dependent energy gap), which is the collective coordinate of most importance to electron transfer (Marcus, 1956; Warshel and Parson, 1991; Tachiya, 1993), and on the correlation of the difference potential with specific vibrations in the protein. This analysis is used to determine the free energy curves of the two states and their curve-crossing point, the rate of vibrational relaxation, and the vibrational motions that contribute to the electron transfer.

There are substantial experimental data about plastocyanin for use in modeling the potential energy surfaces. X-ray crystallographic structures (Redinbo et al., 1994; Guss et al., 1992) show that in the oxidized state the copper atom is liganded to a cysteine sulfur atom and two histidine nitrogen atoms in a distorted trigonal planar configuration. In addition, a methionine sulfur atom is weakly bound to the copper, completing a distorted tetrahedron (see Fig. 1). The equilibrium configuration of the reduced state (Guss et al., 1986) is only slightly displaced (the optically excited state equilibrium configuration, of course, cannot be established by x-ray diffraction). Resonance Raman spectra (Woodruff et al., 1988; Blair et al., 1985; Fraga et al., 1996; Qiu et al., 1995) show several strong peaks around 400 cm^{-1} that have been attributed to the Cu-S(cys) stretch (distributed among several normal modes); a smaller peak near 270 cm^{-1} is attributed to the Cu-N(his) stretches. Absorption spectra show a bright optical transition around 600 nm as well as several less intense transitions (Solomon et al., 1980; Gewirth and Solomon, 1988). Semiempirical electronic structure calculations (Gewirth and Solomon, 1988; Guckert et al., 1995; Larsson et al., 1995) have examined the oxidized, reduced, and excited states. The optical excitation is formally a cysteine $S\pi \rightarrow Cu\ d_{x^2-y^2}$ transition. However, both orbitals are highly mixed, with about 54% Cu and 38% Cys contribution to each, according to self-consistent field-X α -scattered wave (SCF-X α) calculations (Guckert et al., 1995). Thus there is no evidence for the transfer of an electron over any distance or for significant charge redistribution (see also Larsson et al., 1995).

There has been a previous MD simulation of plastocyanin, but with a rather different focus. Wang et al. (1994) used the GROMOS force field with electrostatic (but not bonded) interactions between the copper and protein in an MD study of the effects of solvation on the protein structure and dynamics. In addition, Qiu et al. (1994) and Urushiyama and Tobar (1990) derived multidimensional har-

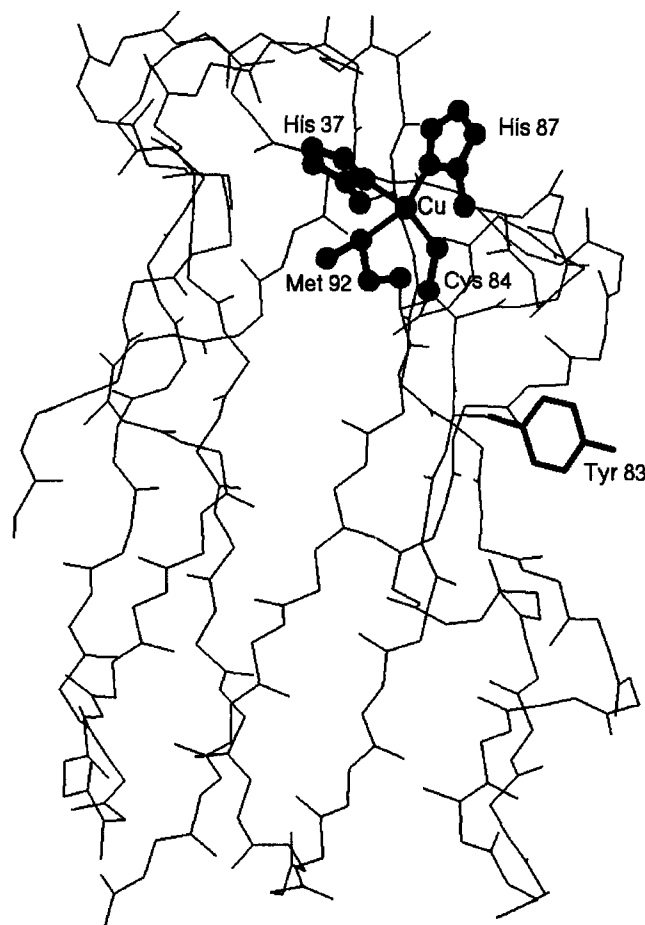


FIGURE 1 The copper center of plastocyanin, showing the copper in a distorted tetrahedral configuration with a cysteine residue, two histidine residues, and a less tightly bound methionine residue. See Table 3 for values of the bond lengths and angles. The figure also shows the protein backbone and the tyrosine 83 side chain, which is thought to be important in electron transport.

monic models of the copper center of the protein and used the normal modes to explore the atomic motions. Perhaps closer in spirit to the present investigation are MD simulations of the vibrations associated with electron transfer in the photosynthetic reaction center (Marchi et al., 1993; Treutlein et al., 1992; Schulten and Tesch, 1991; Creighton et al., 1988). Both equilibrium and nonequilibrium simulations showed the behavior of the energy gap between the excited special pair (P^*BH) and charge-separated (P^+B^-H and P^+BH^-) states.

The structure of this paper is as follows. The next section describes in detail how the molecular mechanics parameters were obtained for the copper-protein interaction and also sets forth other aspects of the model and simulation method. Then several results of the classical dynamics simulations are described, including free energies, time-dependent correlation functions and averages of the difference potential, spectral densities of atomic motions, and the correlation of atomic motions to the electron transfer coordinate. The last section draws conclusions and describes future work.

THE MODEL

Modeling of the blue copper protein

Because of the complexity of proteins, simulations of them usually employ simple forms for the potential energy surface. Here plastocyanin is modeled with a standard molecular mechanics potential, a sum of two-, three-, and four-atom terms. The local interactions include harmonic bonds, angles, improper torsions, and dihedral angles. The long-range interactions include Lennard-Jones van der Waals potentials and electrostatic potentials between atom-based partial charges (Brooks et al., 1983):

$$V = \sum k_r(r - r_0)^2 + \sum k_\theta(\theta - \theta_0)^2 + \sum k_\omega(\omega - \omega_0)^2 + \sum |k_\phi| - k_\phi \cos(n\phi - \phi_0) + \sum_{\text{excl}} \left(\frac{A_{ij}}{r_{ij}^{12}} - \frac{B_{ij}}{r_{ij}^6} \right) + \sum_{\text{excl}} \frac{q_i q_j}{r_{ij}} \quad (1)$$

Several complete, self-consistent, and well-tested sets of parameters for protein atoms have been published based on extensive experimental data and ab initio and semiempirical electronic structure calculations with small model compounds. Parameters for protein atoms in this work are taken from the all-atom sets in CHARMM22 (Brooks et al., 1983). Much less work has been done on transition metals and their interactions with proteins (Wampler, 1994; Hoops et al., 1991; Vedani and Huhta, 1990). Fewer experimental data are available on metal compounds, and most semiempirical methods are not parameterized for copper. In addition, the interactions with partly filled d-orbitals are complicated and often system-specific. Thus it is not clear that general molecular mechanics parameters for copper would be useful, should one go to the effort to derive them. Yet there has been some success in modeling specific metalloproteins (Wang et al., 1994; Merz et al., 1991; Shen and McCammon, 1991). Depending on the flexibility desired at the metal site, these simulations have used bonded or solely electrostatic interactions, often based on x-ray crystal structures and electronic structure calculations of the protein to be modeled.

Here, too, the poplar plastocyanin copper center will be modeled based on known information about the protein. Although no attempt is made to determine generic copper parameters, the method used here should be transferable to other blue copper proteins. Added parameters are chosen, based on the CHARMM parameter sets, for consistency with crystallographic data and with resonance Raman spectra. Because of the strength of the copper interaction with the cysteine and histidine ligands, and because the vibrations are of central importance, the copper is considered to be bound to those three ligands. The interaction with the methionine residue is much weaker, however, and will be modeled using nonbonded interactions. This approach also allows accurate modeling of the very different copper-sulfur interactions without artificially defining different sulfur

types for the cysteine and methionine residues. The plastocyanin simulated here contains 99 amino acid residues and 1443 atoms.

Ground-state parameters

A detailed description of the method for determining each parameter type is given below. The parameters used in the simulations are listed in Tables 1 and 2. A comparison of the average of key internal coordinates in the ground-state equilibrium simulations (described below) with those in the reference crystal structure of poplar plastocyanin (Guss et al., 1992) is given in Table 3.

Partial charges

The formal charge of the copper ion in the oxidized state of plastocyanin is +2 (the copper center including ligands has a +1 charge, as the ligand cysteine has a -1 formal charge). However, the charge is dispersed among the copper ligands, requiring determination of the partial charges on the ligand residues as well as on the copper. These partial charges are not rigorously defined physical quantities; they are param-

TABLE 1 Copper-protein interaction parameters added to the CHARMM22 all-atom protein parameter set

	Bonds		
	r_0	k_r	
Cu-S*	2.10 Å (excited: 2.40)	110 kcal/mol Å	
Cu-N	2.05	110	
Angles			
	θ_0	k_θ	
Cu-S-C	95°	15 kcal/mol	
Cu-N-Cph1	130	20	
Cu-N-Cph2	126	20	
S-Cu-N	130	20	
N-Cu-N	100	20	
Dihedral angles			
	ϕ_0	k_ϕ	n
Cu-S-C-C#	0°	0.24 kcal/mol	1
Cu-S-C-C	0	0.15	2
Cu-S-C-C	0	0.27	3
Cu-S-C-H	0	0.20	3
Cu-N-C-C	180	1.00	2
Cu-N-C-H	180	1.00	2
Cu-N-C-N	180	1.00	2
Improper torsions			
	ω_0	k_ω	
N-C-C-Cu	0°	0.45 kcal/mol	
Cu-S-N-N	0	3.50	
Cu-N-S-N	0	3.50	
Cu-N-N-S	0	3.50	
van der Waals interactions			
	r_{\min}	E_{\min}	
Cu	1.09 Å	0.25 kcal/mol	
Cu-O	4.50	0.10	

* Unless otherwise specified, atoms refer to all atom types of the designated element.

Note that some dihedral angles have multiple terms in the potential.

TABLE 2 Atomic partial charges for copper and ligand residues used in the molecular mechanics potential

	Copper	Cysteine	Histidine			
Cu	0.98 <i>e</i>	S	-0.43 <i>e</i>	N _{δ1}	-0.62 <i>e</i>	
		C _β	-0.21	C _γ	0.22	
				C _β	-0.08	
				C _{δ2}	0.05	H _{δ2} 0.11 <i>e</i>
				N _{ε2}	-0.42	H _{ε2} 0.37
				C _{ε1}	0.28	H _{ε1} 0.15
Residue*	0.98	-0.46			0.24	

* Totals are for whole residues (including unchanged backbone and hydrogen atom charges).

eters in an approximate potential energy surface, chosen in conjunction with other parameters to model interatomic forces. Thus the prime criterion for choosing partial charges is not the accuracy of an electronic structure calculation, but the accuracy of the full potential energy surface, including preset CHARMM protein parameters. Although derivation of charges from ab initio calculations as similar as possible to those used in developing the CHARMM potential function would be ideal, a simpler method is used here. To ensure consistency with the existing protein potential, partial charges of the protein atoms in the copper ligand residues are linearly interpolated between the standard CHARMM charges of the corresponding atoms in the protonated and unprotonated residues (with CHARMM names CYS and methylthiolate MES1 for cysteine, HSP and HSE for histidine); the interpolation point is determined by comparing the full copper-center residue partial charge to the charge of the unprotonated residue and the partial charge of the protonated residue without the extra hydrogen.

With this ansatz it is necessary only to determine the residue and copper ion charges; small inaccuracies, when

TABLE 3 Comparison of copper center structure between x-ray crystal structure, ground-state simulation average, and excited state simulation average

	Crystal	Ground avg.	Excited avg.
Distances			
Cu-S(cys)	2.067 Å	2.073 Å	2.364 Å
Cu-N(his87)	2.059	1.998	1.995
Cu-N(his37)	1.906	1.986	1.981
Cu-S(met)	2.822	2.918	2.836
Cu-O(pro)	3.888	3.925	3.855
Angles			
S(cys)-Cu-N(87)	121°	128°	128°
S(cys)-Cu-N(37)	132	126	125
N(87)-Cu-N(37)	97	92	94
S(cys)-Cu-S(met)	110	110	106
Dihedral angles			
C _β (cys)-S(cys)-Cu-S(met)	3°	8°	9°
C _γ (87)-N(87)-Cu-S(met)	77	65	64
C _γ (37)-N(37)-Cu-S(met)	112	136	131
Improper torsions			
Cu-S(cys)-N(87)-N(37)	21°	28°	28°
Cu-S(cys)-N(37)-N(87)	27	27	26
Cu-N(87)-N(37)-S(cys)	16	17	9

spread over the whole residue and compensated by experimentally determined parameters, should not have much effect. An AM1 (Dewar et al., 1985) semiempirical calculation of the copper with the three ligand side chains in a configuration taken from the crystal structure was done for this purpose using the program Spartan (Wavefunction, Inc.). Because copper is not parameterized in AM1 (or similar semiempirical methods) a zinc II ion was substituted. Charges were derived from an electrostatic potential fit. For simplicity, the average of the charges on the two histidine residues was used for both, and the backbone charges were left unchanged. The resulting charges are tabulated in Table 2. Comparable calculations including the methionine side chain added less than 0.1*e* to the rest of the metal center.

Lennard-Jones parameters

The Lennard-Jones parameters are difficult to determine experimentally, and again consistency with other parameters is an important criterion. Thus the CHARMM parameters for Zn were used unchanged. However, in simulations it was found that the proline 36 tended to move much closer to the copper ion than is found in crystal structures, displacing the methionine and rearranging the copper center; the attraction was due to electrostatic interactions between the pro O and the Cu. To prevent this, an ad hoc Cu-O van der Waals interaction was added to keep the proline at an appropriate distance.

Bond, angle, and torsion equilibria

The parameters for angles and torsions in which the copper ion takes the place of a hydrogen at one end were taken from the protonated residue parameter sets (replacing the hydrogen with the copper). The angle and dihedral equilibria that determine the configuration of the ligands around the copper were set to typical values and adjusted, if necessary, to match ground-state molecular dynamics simulations to the crystal structure. For example, semiempirical electronic structure calculations suggest that the three ligands optimally would be planar around the copper ion; thus the three improper torsion equilibria around the copper are set to zero. The bond equilibria were iteratively adjusted with the force constants (see below), so that the averages of the bond distances in MD simulations were close to the crystal structure values.

Bond, angle, and torsion force constants

The angle and dihedral force constants were set to typical values, again using parameters from protonated residues and from other metals, and adjusted to reproduce the crystal structure. The bond force constants were set so that the frequencies in the spectral densities of the simulated bond distance autocorrelation functions (described in the Results section) would match the observed resonance Raman fre-

quencies (Blair et al., 1985) of approximately 400 cm^{-1} for the Cu-S(cys) bond and 270 cm^{-1} for the Cu-N(his) bonds. The force constants used are considerably stronger than those derived for small copper compounds by Bernhardt and Comba (1992).

As shown in Table 3, the average structure of the copper center is close to that determined experimentally by x-ray crystallography. The structure fluctuates in simulations but does not drift significantly over hundreds of picoseconds. The similarity to the experimental structure cannot be taken as independent proof of the accuracy of the model, but rather is a measure of the care taken in matching the target. The model will be tested by comparison of simulation results to other experiments, including ongoing work by L. D. Book et al. in ultrafast spectroscopy (Scherer et al., 1996).

Modeling the excited state

An excited-state potential energy surface is needed both for simulations after optical excitation and to determine the potential difference between the electronic states. This difference potential is the “reaction coordinate” or electron transfer coordinate. Modeling the excited state is difficult, as there is no experimental information on this state beyond what can be derived from the absorption spectrum and from preliminary fluorescence (Fraga et al., 1996) and pump-probe (Scherer et al., 1996) measurements. The most obvious way of modeling a charge transfer state would be to change the partial charges of the copper ion and surrounding residues. However, semiempirical electronic structure calculations using both SCF- $X\alpha$ -SW (Guckert et al., 1995) and CINDO/S (Larsson et al., 1995) methods suggest that there is no net motion of charge between atoms upon excitation. In the SCF- $X\alpha$ calculation, for example, the initial “S(cys) $n\pi^*$ ” orbital and the final “Cu $d_{x^2-y^2}$ ” orbital have almost identical Mulliken populations on the Cu (54%) and S (35–36%) atoms. The calculations do show, however, that the electronic excitation is localized around the Cu and S(cys) atoms, so the change in the potential should be greatest for the Cu-S(cys) bond.

Therefore, in modeling of the excited state the partial charges are not changed from the ground state. The sole difference between the two potentials, besides a constant electronic energy gap, is chosen to be an increase in the equilibrium bond length (r_0) in the harmonic Cu-S(cys) interaction (while the force constant also could change, as suggested by preliminary analysis of wavelength-resolved pump-probe data (Scherer et al., 1996), there is not yet sufficient basis to estimate a new value). This choice is particularly convenient in that the difference potential ΔV is directly proportional to the Cu-S(cys) bond distance x (apart from a constant factor):

$$x = |\mathbf{r}_{\text{Cu}} - \mathbf{r}_{\text{S(cys)}}|, \quad (2)$$

$$\Delta V = V_{\text{exc}} - V_{\text{gnd}} = 2k_x d(x - \bar{x}) + \epsilon, \quad (3)$$

where $d = x_{0,e} - x_{0,g}$, $\bar{x} = (x_{0,e} + x_{0,g})/2$, and $x_{0,g}$ and $x_{0,e}$ are the minima for the Cu-S(cys) interaction in the respective states. Because of its direct proportionality to the difference potential, the coordinate x will be used as the electron transfer coordinate.

The magnitudes of both the Cu-S(cys) minimum shift d and the energy shift ϵ can be estimated by a comparison of the observed and simulated absorption spectra (Hush, 1967). Gaussian decomposition of the observed spectrum of bean plastocyanin (Solomon et al., 1980) at 270K yielded for the charge transfer optical transition a peak frequency of $16,500\text{ cm}^{-1}$ and a FWHM of 2602 cm^{-1} . After adjusting for an approximate $T^{1/2}$ dependence of the spectral width (based on a classical displaced harmonic system), the spectral width at room temperature $\Delta\omega = \text{FWHM}/(8 \ln 2)^{1/2} = 1165\text{ cm}^{-1}$. The absorption spectrum from classical simulations, as described in the Results section, takes the same peak frequency for an added energy gap between the states of $\epsilon = 12,500\text{ cm}^{-1}$ and the same spectral width for a Cu-S(cys) displacement of $d = 0.295\text{ \AA}$. Thus the excited-state simulations described below use a minimum for the Cu-S(cys) interaction of 2.40 \AA .

The average values of selected internal coordinates in the excited-state equilibrium simulations are given in Table 3. There appears to be very little restructuring in the excited state in this model, except for the Cu-S(cys) distance. The spectral density of x in the excited state (see Eq. 10) also is close to that in the ground state, with peak positions varying by no more than the 3 cm^{-1} resolution. By not taking into account any difference potential contributions from other coordinates, this calculation may somewhat overestimate the actual displacement in this one coordinate and underestimate others. Nonetheless, it is the best estimate from available data.

Protein environment

Solvation in water has been shown to have a significant impact on both the structure and the dynamics of proteins (van Gunsteren et al., 1994; Brooks et al., 1988). The main focus of this paper, however, is on the copper center of plastocyanin, and the copper ion is shielded from the solvent on all sides. In particular, the electronic transition being studied is localized in the copper center and does not involve charge transfer over a long distance. Thus the solvent should have a limited impact on the results presented below. The simulations included 109 water molecules with positions identified in the crystal structure, but they included no other solvent. The water molecules were modeled with the rigid TIP3 potential.

The crystallographic solvent molecules should include those with the strongest interaction with the protein and should model the most important specific protein-solvent interactions, but the general solvent heat bath, caging, solvation, and stochastic effects may not be well modeled. In particular, a more complete solvent environment could dis-

sipate coherent motions of atoms on the protein surface that are shown below. Although charge screening of ionizable groups is only partial in this model, these charges do not change in the process studied and should have limited impact. In any case, the qualitative features of the free energy curves described below are constrained by experimental data. Previous MD simulations of plastocyanin solvated by 44 to 2516 water molecules (with a somewhat different potential) found the most compact protein structure and smallest fluctuations, but relatively large deviation from the crystal structure, with 80 solvent molecules included (Wang et al., 1994). These results suggest that better solvation could also loosen the protein structure somewhat. However, the vibrational correlations with the localized excitation buried in the protein should be less affected by the solvent than the fluctuations studied by Wang et al.

Also in keeping with the focus on the copper center, the semisolvated protein was isolated in space; no periodic boundary conditions, walls, or Ewald summation were used. The long-range potential cutoff was set to the CHARMM recommended value of 12 Å. Despite the lack of boundaries, no denaturing or loss of solvent molecules was observed during the simulations.

Classical molecular dynamics simulation methods

The molecular mechanics potential that has just been described was used in a series of classical MD simulations using CHARMM23 (Brooks et al., 1983). All simulations were conducted in a microcanonical ensemble (i.e., without a thermostat), which was judged most trustworthy for the dynamical information that was sought. In all cases the temperature was initially equilibrated to 300K, the time step was 1 fs, data were collected every 5 fs, and bonds to hydrogen atoms were fixed with SHAKE (Ryckaert et al., 1977).

The first set of simulations investigated nuclear fluctuations in the equilibrium distribution of the oxidized ground state. Starting from the crystallographic structure (Guss et al., 1992), the potential was minimized to a local minimum, and then the structure was equilibrated for 268 ps with periodic rescaling of the velocities. Data were collected over 15 runs; each started from the final configuration of the previous run with velocities randomly assigned from a Boltzmann distribution; reassignment of velocities was used for better sampling of the phase space. The system was reequilibrated for 7 ps and data were collected for 40 ps. Long-term fluctuations were observed in the potential energy, and the average potential varied considerably between runs, but without an apparent pattern. The difference potential ΔV fluctuated around a constant value that showed no long-term correlation.

The second set of simulations followed average nuclear motions in the excited state, starting from an equilibrium distribution in the ground state. The dynamics in the excited

state were followed for 5 ps starting from 110 randomly selected phase points (both coordinates and momenta) from the ground-state equilibrium simulations. The third set of simulations was conducted in equilibrium in the excited state, in a manner identical to the first set, but for only 10 runs.

Several analyses of the MD simulation results are described in the following section.

RESULTS AND DISCUSSION

Probability distributions and free energies

The multidimensional potential energy surfaces can be explored using the equilibrium distributions determined in the simulations. To determine the coordinate and energy displacements between the ground and optically excited states, the probability distribution of the potential difference between the states can be compared to the experimental absorption spectrum for the system. The probability distribution in each state can then be used to determine free energy curves. As noted above, the Cu-S(cys) distance x will be used to represent the difference potential, to which it is proportional (see Eq. 3).

The probability distribution of x near the ground-state equilibrium (Tachiya, 1993) can be found by binning points from the first set of simulations:

$$P(x_0) \equiv \langle \delta(x - x_0) \rangle \equiv \frac{\text{Tr}[e^{-V_{\text{gnd}}/k_B T} \delta(x - x_0)]}{\text{Tr}[e^{-V_{\text{gnd}}/k_B T}]}, \quad (4)$$

where $\langle \dots \rangle$ is a classical equilibrium average. The electronic absorption spectrum (McQuarrie, 1976) under the Condon approximation,

$$I(\omega) \propto \frac{1}{2} \int_{-\infty}^{\infty} dt e^{i\omega t} \langle e^{iH_{\text{gnd}}t/\hbar} e^{-iH_{\text{exc}}t/\hbar} \rangle, \quad (5)$$

where H_{gnd} and H_{exc} are the Hamiltonians in the respective states, reduces for a classical system to the probability distribution of the difference potential:

$$I(\omega) \propto \langle \delta(\omega - \Delta V) \rangle. \quad (6)$$

Matching the first and second moments of the observed and simulated spectra, as described in the section on modeling the excited state, requires an energy displacement of 12,500 cm^{-1} and a coordinate displacement in x of 0.295 Å. In the excited-state potential a minimum of $x_0 = 2.40$ Å was used, for which the corresponding energy displacement $\epsilon = 12,400 \text{ cm}^{-1}$.

Free energy curves for x are easily found from the probability distributions in the ground and excited states (Allen and Tildesley, 1987):

$$P(x_0) = \exp[-F(x_0)/k_B T + \text{constant}]. \quad (7)$$

The free energy difference is equal to the difference potential, $F_{\text{exc}}(x) - F_{\text{gnd}}(x) = \Delta V(x)$. In Fig. 2 the free energy

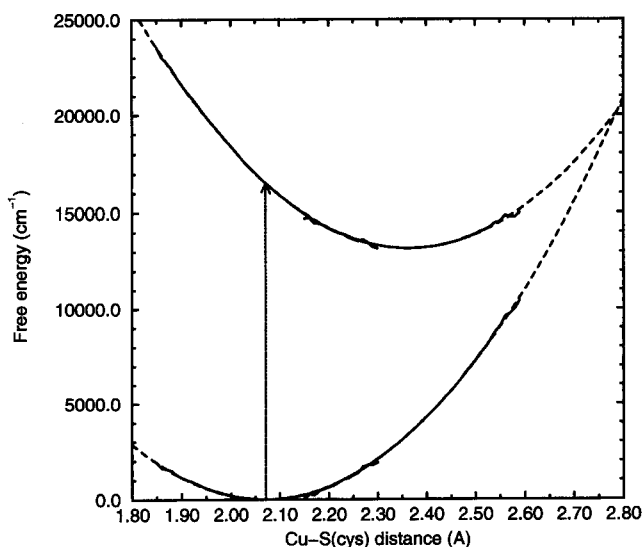


FIGURE 2 Free energy curves for the ground and optically excited charge-transfer states determined from equilibrium simulations in the two states (see Eq. 7). The dashed lines are harmonic fits to each curve. The vertical arrow indicates vertical optical excitation from equilibrium, which is the maximum of the absorption spectrum. The states are well within the Marcus inverted region.

curves from simulations in the two equilibrium distributions are matched to eliminate the undetermined constant, and the combined curves are fit to harmonic approximations. The noise at the edges of the curves is due to poor sampling of those infrequently occurring configurations. The simulations yield a difference between the free energy minima of $13,200\text{ cm}^{-1}$, corresponding to a “solvation” or reorganization energy in the excited state of 3300 cm^{-1} . The parabolic fits to the free energies are excellent, as they have been in other biological simulations (Marchi et al., 1993; Warshel et al., 1992), suggesting that theories based on collective harmonic approximations (including Marcus theory) could be valid for this system.

The free energy curves are well within the Marcus inverted region, with an intersection at $x = 2.80\text{ Å}$, which is beyond the region accessed in thermal equilibrium in either state. The potential energy at the intersection is, in the harmonic approximation, $20,200\text{ cm}^{-1}$, 3700 cm^{-1} above the vertical transition from the ground-state minimum. Although the simplified difference potential probably overestimates the displacement in the Cu-S(cys) coordinate, the placement of the curves well into the inverted region should be correct. The small coordinate displacements between the two states reflect the small differences that were found from x-ray crystallography of the reduced and oxidized states, with a Cu-S(cys) distance of 2.16 Å and Cu-N(his) distances of 2.37 and 2.15 Å in the reduced state for pH 7.0 (Guss et al., 1986). The small displacements facilitate natural electron transfer as long as the energies of the states are similar.

However, the energy gap between the oxidized and optically excited states makes their intersection inaccessible and thus makes electron transfer back to the ground state

difficult. The high energy of the intersection, combined with the narrow gap between the potential curves in the inverted configuration (see Fig. 2), suggests that tunneling between the states rather than nonadiabatic transfer at the curve crossing is likely to be important in the back electron transfer. The inclusion of tunneling in future calculations of the back electron transfer rate will be discussed in the Conclusions.

The displacement of the potentials in this model is apparently somewhat greater than that found by Fraga et al. (1996) for parsley plastocyanin. They measured a difference between absorption and fluorescence maxima of 2700 cm^{-1} and from resonance Raman data estimated a reorganization energy of 2000 cm^{-1} . The relatively small energy differences suggest that the coordinate displacement of the potentials is small and thus that the curve crossing is too high in energy to be accessible. The authors attribute the 20-fs excited-state lifetime they derive to relaxation via lower-lying ligand-field states.

Vibrational relaxation

In addition to generating the equilibrium ensembles used in the previous subsection, classical MD simulations can follow the vibrational dynamics associated with electron transfer in real time. The vibrational motion in the excited state after a very short pulse is illustrated in Fig. 3 a, which shows the nonequilibrium time-dependent average of the Cu-S(cys) distance (or difference potential) for the ground-state thermal equilibrium propagated in the excited-state potential:

$$\bar{x}(t) = \langle x(t)_{exc} \rangle. \quad (8)$$

The average shows large, periodic oscillations in the Cu-S(cys) bond due to the largely harmonic interaction potential. The oscillation decays nonexponentially because of coupling to many other coordinates (see the subsection on protein atomic motions). The vibrational relaxation mostly occurs within 0.5 ps and is largely over within 2.5 ps. If the curve crossing with the ground state lies high in the excited well, as found earlier, this fast relaxation could cause the back electron transfer rate to be large and periodic for a few oscillations, then thermal and slow afterward.

It should be noted that the oscillations in the difference potential may be somewhat overemphasized, both by its simplified representation and by the lack of anharmonicity in the bond interaction model. Thus the vibrational relaxation rate could increase somewhat for a more complicated and realistic difference potential. In addition, the inclusion of a solvent could increase the damping, although the effect should be small.

Vibrational dynamics in the ground state can be probed using an equilibrium two-time correlation function of the coordinate x (here the equilibrium and the dynamics are both in the ground electronic state) (Allen and Tildesley, 1987):

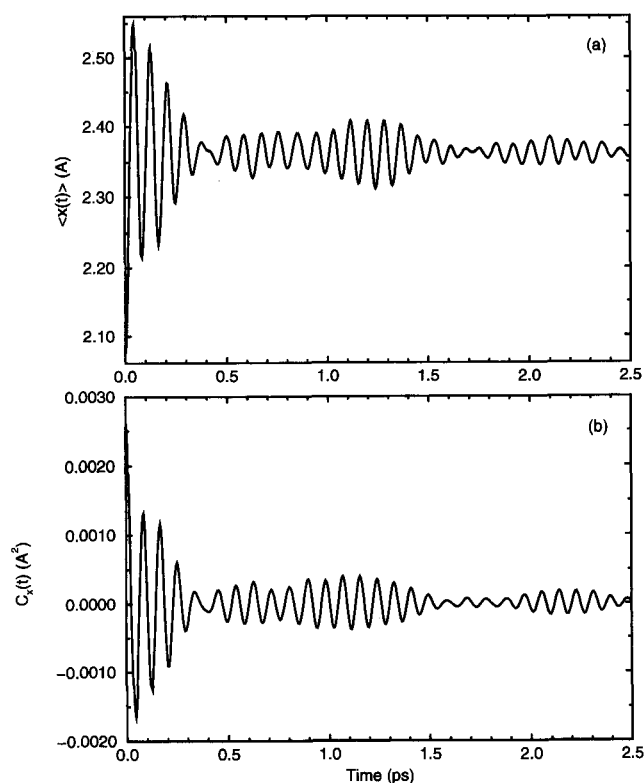


FIGURE 3 (a) The nonequilibrium average of the Cu-S(cys) distance x (which is proportional to the difference potential) for ground-state thermal equilibrium propagated in the excited state (see Eq. 8). (b) The equilibrium two-time correlation function of x in the ground state (see Eq. 9). The signal decay rates indicate the vibrational relaxation rates in the respective states. The similarity of the two graphs is a measure of linear response.

$$C_x(t) = \langle x(t)x(0) \rangle - \langle x \rangle^2. \quad (9)$$

The function $C_x(t)$ is shown in Fig. 3 *b*. Again, the strong oscillations decay in 0.5–2.5 ps. This decay is in semiquantitative agreement with the relaxation times in pump-probe measurements of ground-state modes in the 400 cm^{-1} region (Scherer et al., 1996). The striking similarity of the nonequilibrium average and the equilibrium correlation function (if one of them is flipped about a horizontal axis) shows that the response of this system is linear, i.e., that the photoinduced large-amplitude motions are linearly related to extensions of the small equilibrium fluctuations and that the dynamics are similar in the ground and excited states. Correlation functions from equilibrium simulations in the excited electronic state (not shown) confirm this similarity. As the structural difference between the two states is both simple and small, the success of linear response is not surprising, but again it suggests that a displaced harmonic model could be successful.

Vibrational frequencies and modes

Whereas the difference potential is simply proportional to the Cu-S(cys) distance in this model, the rest of the potential couples other protein motions to this central coordinate. The

specific protein vibrations that are coupled to the electron transfer can more easily be analyzed in the frequency domain. Taking the Fourier transform of the correlation function $C(t)$ yields a spectral density:

$$C(\omega) = 2 \int_0^{\infty} dt \cos(\omega t) C(t). \quad (10)$$

The spectral density $C_x(\omega)$ of the Cu-S(cys) distance, shown in Fig. 4, shows many unresolved low-frequency modes and several larger peaks near 400 cm^{-1} . It is similar to the resonance Raman spectrum, which for photoinduced electron transfer systems also reflects vibrational motions that are coupled to and displaced upon charge transfer (Myers, 1994). Indeed, as described in the section on the model, the copper-ligand stretch frequencies of roughly 270 and 400 cm^{-1} were fit to Raman data. Like the resonance Raman spectrum of plastocyanin (Woodruff et al., 1988; Blair et al., 1985; Fraga et al., 1996; Qiu et al., 1995), the calculated spectral density exhibits two major peaks that are split around 400 cm^{-1} , with smaller peaks forming a higher frequency shoulder. There is a small peak near 260 cm^{-1} , but it is smaller than the corresponding peak observed in the Raman spectrum. The cysteine S-C stretch, to which the experimentally observed small peak at 765 cm^{-1} has been attributed (Fraga et al., 1996), vibrates at 730 – 750 cm^{-1} in the simulation but leaves only infinitesimal peaks in $C_x(\omega)$. The broad Raman intensity near 800 cm^{-1} attributed to combination bands is not apparent in the simulated spectral density. The breadth of this signal is taken as evidence of strong Duschinsky mixing (Blair et al., 1985), which would require a more complicated difference potential to simulate.

Although vibrations at many frequencies clearly are coupled to the electronic transition, it is not clear how to describe these vibrations in terms of specific atomic motions. Previous analyses found normal modes for a large part of the protein around the copper center (Urushiyama and

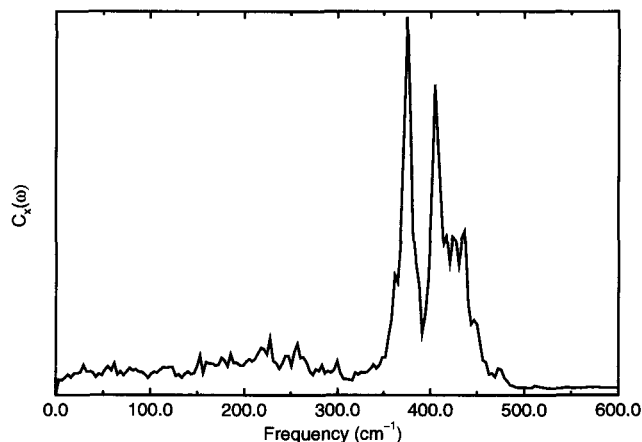


FIGURE 4 The spectral density of the Cu-S(cys) distance x correlation function in the ground state (the Fourier transform of Fig. 3 *b*). The difference potential spectral density is identical in this model.

Tobari, 1990) and for a smaller analog compound (Qiu et al., 1994) from potentials consisting only of harmonic bonded interactions, but the sheer number of coordinates makes such an analysis unwieldy, and the anharmonicity of the actual plastocyanin potential challenges its accuracy. Here a different method will be used, focused more narrowly on the residues liganded to the copper ion: the spectral density of the key coordinate x will be compared with spectral densities from the autocorrelation functions of other internal coordinates and with Fourier transforms of the cross-correlation functions of the internal coordinates q_n with x :

$$C_{x_n}(\omega) \quad (11)$$

$$= 2 \int_0^{\infty} dt \cos(\omega t) \frac{1/2 \langle x(t)q_n(0) + q_n(t)x(0) \rangle - \langle x \rangle \langle q_n \rangle}{(\langle x(t)x(0) \rangle - \langle x \rangle^2)^{1/2} (\langle q_n(t)q_n(0) \rangle - \langle q_n \rangle^2)^{1/2}}$$

The spectral densities of the Cu-N(his) bond lengths are shown in Fig. 5 along with the Fourier transforms of the cross-correlations with x ; the spectral density of x is shown for comparison. The primary frequency of the bond stretches is the same in both cases (a single force constant was used for both harmonic interactions), corresponding with a small peak in $C_x(\omega)$. The cross-correlation of Cu-N(his87) with x is an almost identical but inverted copy of $C_x(\omega)$ for the peaks near 400 cm^{-1} . The peaks are negative because the Cu-N bond shortens while the Cu-S bond

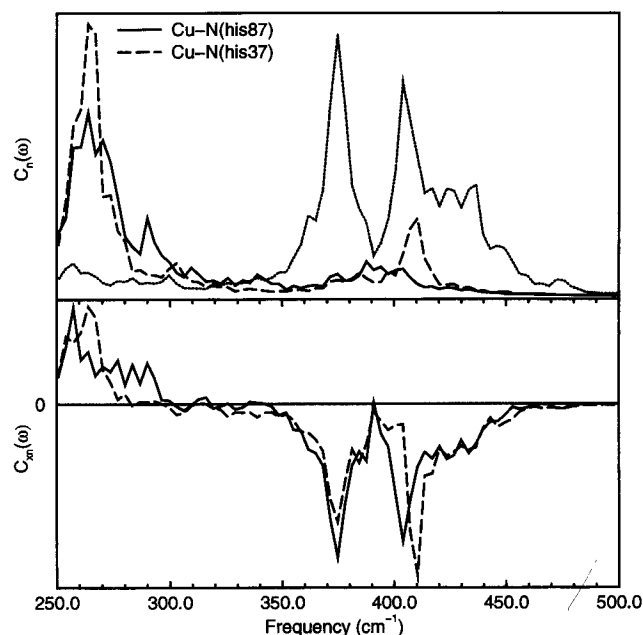


FIGURE 5 The upper panel shows the spectral densities of the Cu-N(his87) (solid) and Cu-N(his37) (dashed) bond lengths. The corresponding lines in the lower panel are the Fourier transforms of the cross-correlation functions with x (on a different scale). The fainter dotted line is $C_x(\omega)$ from Fig. 4 for comparison. The correlation with x occurs primarily because in the Cu-S(cys) stretch the Cu atom moves toward the histidines.

lengthens (the bond lengths are anticorrelated) during motions at these frequencies. The similarity of the spectra suggests that the correlation is similar for all motions of the Cu-S bond—if the Cu moves away from the S(cys), it will move toward the histidine nitrogens. The cross-correlation of Cu-N(his37) also follows $C_x(\omega)$, but both the auto- and cross-correlation spectra show enhanced peaks at 410 cm^{-1} .

Peaks in essentially all of the copper-center cross-correlation spectra at 375 cm^{-1} can be explained by motion of the Cu atom away from the S(cys) atom with very little protein motion. There is a slight contraction of the histidine rings, but essentially no correlation with cysteine motion. There may be some overlap with Cu-N(his87)-C(his87) bends at 390 cm^{-1} . Thus the largest peak in the difference potential spectral density appears to be a relatively “pure” Cu-S(cys) stretch.

The $C_x(\omega)$ peak at 405 cm^{-1} is clearly due to motion of both the Cu and the S(cys) atoms. Their stretch appears to be mixed with the motion of the histidine 37 as S(cys)-Cu-N(his37) and both Cu-N(his37)-C(his37) angle spectral densities (not shown) also show strong peaks at 405 cm^{-1} . There appears to be a different mode at 410 cm^{-1} ; e.g., the S(cys)-Cu-N(his37) cross-correlation is negative at 405 cm^{-1} but is positive at 410 cm^{-1} .

The smaller peaks in $C_x(\omega)$ around 415, 425, and 435 cm^{-1} are strongly mixed with cysteine motions. Most of the auto- and cross-correlation spectra show no amplitude in this region, but the cross-correlations of the S(cys)-C(cys) bond, the Cu-S(cys)-C(cys) angle, and the C(cys)-S(cys)-Cu-S(met) dihedral angle with x all show relatively strong negative peaks corresponding with the peaks in $C_x(\omega)$, as shown in Fig. 6. The spectral density of the Cu-S(cys)-C(cys) angle also has unusually large peaks in this region.

Protein atomic motions coupled to electron transfer

The coupling between nuclear motions does not stop with the ligand residues. Precisely which protein motions are strongly coupled to the electronic transition can be seen from the cross-correlation function of the Cartesian motions of each protein atom with the reaction coordinate:

$$C_{x_i,\alpha} = \frac{\langle r_{i,\alpha}x \rangle - \langle r_{i,\alpha} \rangle \langle x \rangle}{(\langle r_{i,\alpha}^2 \rangle - \langle r_{i,\alpha} \rangle^2)^{1/2} (\langle x^2 \rangle - \langle x \rangle^2)^{1/2}}, \quad (12)$$

where i designates the atom and α designates one of the three atomic coordinates. The geometrical average of $C_{x_i,\alpha}$ for each atom gives a single atomic parameter: $C_{x_i} = (\sum_{\alpha} C_{x_i,\alpha}^2)^{1/2}$.

In Fig. 7 the atoms are colored according to the correlation of their motion with the Cu-S(cys) distance. The range from yellow to red corresponds to $C_{x_i} = 0.04$ to $C_{x_i} = 0.10$; the color slowly fades to grey for $C_{x_i} < 0.04$, and atoms are red for $C_{x_i} > 0.10$. The full range of data is from less than 0.005 for distant atoms to 0.16 and 0.13 for the Cu and S(cys) atoms. As is apparent in the figure, the motions of

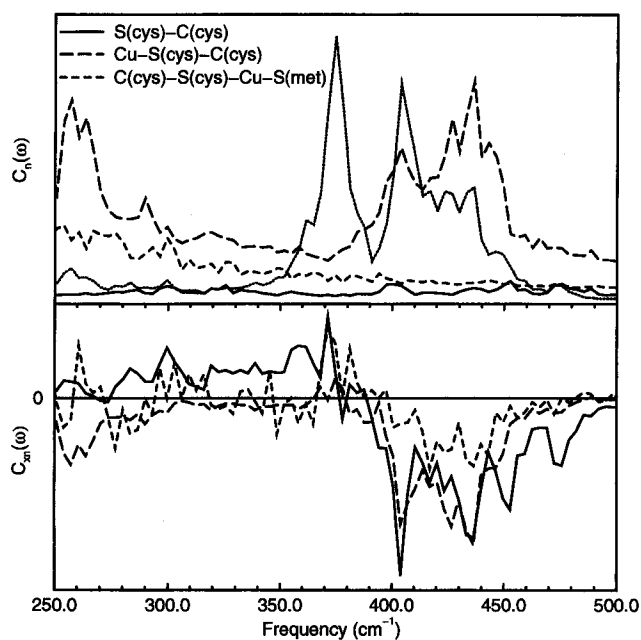


FIGURE 6 The upper panel shows the spectral densities of the $S(\text{cys})\text{-C}(\text{cys})$ bond (solid), $\text{Cu-S}(\text{cys})\text{-C}(\text{cys})$ angle (long dashes), and $\text{C}(\text{cys})\text{-S}(\text{cys})\text{-Cu-S}(\text{met})$ dihedral angle (short dashes). The corresponding lines in the lower panel are the Fourier transforms of the cross-correlation functions with x . The fainter dotted line is $C_x(\omega)$ for comparison. Each graph is scaled separately for visibility. The correlations show that cysteine vibrations are mixed with x in the vibrations from 415 to 435 cm^{-1} .

protein atoms far from the copper center, some more than 20 Å away, are correlated with the electron transfer in this model. The correlation follows the protein backbone from the cysteine residue and to a lesser extent from the two ligand histidines. There is much less correlation across nonbonded interactions: the methionine 92 atoms show $C_{xi} \leq 0.06$, and the residues adjacent to the methionine show still less correlation.

The strength of the correlation over long distances may be surprising, but it is consistent with the protein structure. The protein backbone, both in nature and in the simplified molecular model, contains a repeated series of harmonic bonded interactions with similar force constants in an overall structure that is stable; it is as similar to a crystal as it is to a liquid, in some ways resembling a one-dimensional crystal in solution. Thus long-range vibrations vaguely reminiscent of phonons should exist. Careful comparison of resonance Raman results for different plastocyanins confirms that residues at least 8 Å away from the copper center are coupled directly or indirectly to the optical transition (Loppnow and Fraga, 1996).

The biological function of this striking vibrational correlation is less clear at the present time. Coupling of the electron transfer to some nuclear motions is necessary for the nuclear motions to facilitate the electronic process, as described in the Introduction. Long-range vibrational coupling could make possible relatively large energy fluctuations with many small coordinate displacements that do not

disrupt the protein structure. The correlation certainly should enable efficient damping of vibrations induced by the electron transfer, as seen in the previous subsection. It is possible that directional correlated nuclear motion facilitates a sequence of electron hops or a large motion via superexchange, allowing the electron to travel a long distance from the docking site to the metal center. The directional vibrational coupling could also imply heightened nuclear tunneling in those modes, hence enhancing the overall electron transfer rate.

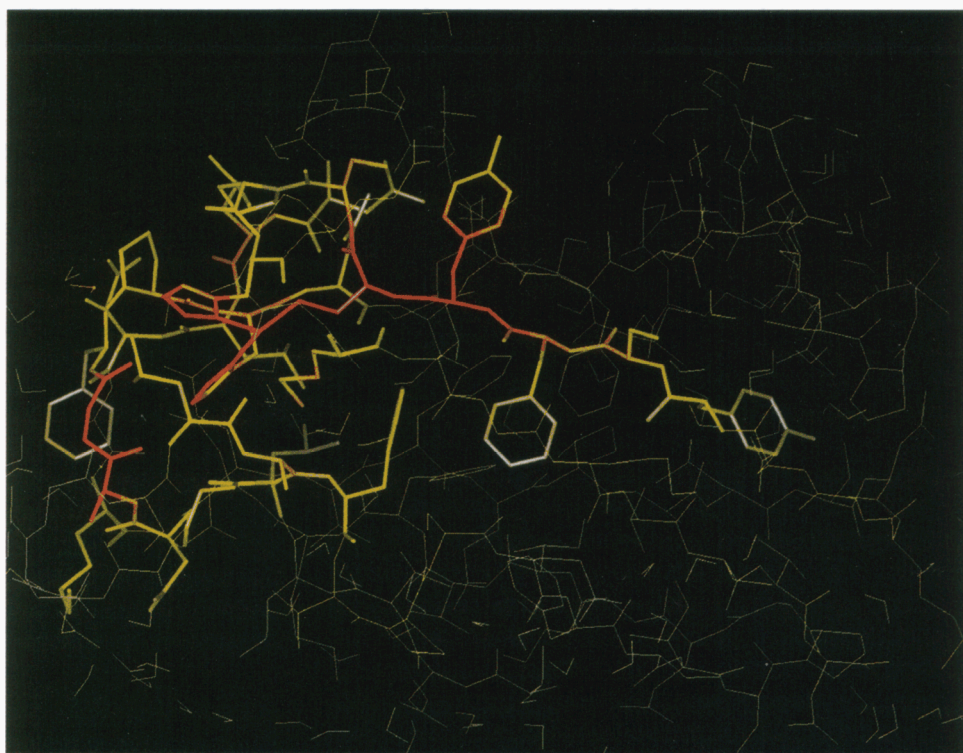
As the vibrational couplings are caused by strong electronic coupling between the atoms, the vibrational correlation could also indicate paths by which long-range electron transfer can occur (i.e., pathways with significant Franck-Condon factors). In the natural function of plastocyanin the electron transferred from cytochrome *f* is proposed to enter through a negative patch on both sides of the prominent tyrosine 83. The transfer to photosystem I seems to occur via a hydrophobic patch with a number of residues surrounding the histidine 87 (Sykes, 1991a; Redinbo et al., 1994; He et al., 1991; Nordling et al., 1991; Modi et al., 1992). As is clear in Fig. 7, the vibrational coupling of both the tyr83 and his87 rings to the $\text{Cu-S}(\text{cys})$ bond is very strong. The coupling to the residues of the hydrophobic patch (e.g., ala33-phe35) also is strong, although the coupling to the negative patch residues other than asp61, which lie up to 20 Å from the copper ion, is somewhat weaker. If the coincidence between vibrational correlation paths and electron transfer paths is more generally valid, then analysis of molecular dynamics simulations could be a relatively easy way of finding important electron transfer pathways without undertaking separate electronic calculations for each possible path, as is done in Onuchic and Beratan's method (Beratan et al., 1992; Onuchic et al., 1992; Curry et al., 1995; Ullmann and Kostić, 1995; Kuki and Wolynes, 1987).

SUMMARY AND CONCLUSIONS

This paper has examined electron transfer dynamics in a protein from a particular perspective: a photoinduced rather than thermal electron transfer process was modeled, and the nuclear rather than electronic dynamics associated with the charge transfer were simulated. The long-term purpose of the research is, in conjunction with ultrafast experiments, to illuminate the electronic and nuclear dynamics of both photoinduced and thermal electron transfer in plastocyanin and other proteins.

A molecular mechanics potential energy surface was used to model plastocyanin after careful calibration to reproduce known experimental data about the copper center. Although the use of data about plastocyanin to parameterize its own model is ad hoc, it promises a more accurate simulation of information that cannot easily be extracted from experiment. Limited comparison with aspects of the crystal structure and minor Raman peaks not used to develop the model

FIGURE 7 The plastocyanin colored to depict the correlation of the atomic motions with the optical electron transfer difference potential. Correlation C_{xi} from 0.04 to 0.1 is colored in a spectrum from yellow to red, with yellow fading to grey for C_{xi} from 0.04 to 0 and with red above 0.1. Residues with any atom having $C_{xi} > 0.04$ are highlighted. Motions of atoms throughout the protein are correlated with the difference potential. The correlation is especially strong along the putative electron transport paths through tyrosine 83 and histidine 87.



suggests that the main features are consistent. Little information is available about the optically excited state, but the simple difference potential, chosen to be proportional to the key Cu-S(cys) bond distance, appears to capture the main nuclear dynamics associated with the optical electron transfer.

Some simulation results will be tested against ultrafast pump-probe experiments. Preliminary experimental results (Scherer et al., 1996) excite a lower energy $d \rightarrow d$ transition that could be coupled to different vibrational modes, but pump-probe experiments that excite the bright optical transition are in progress. Pump-probe spectra can show the frequencies of vibrations in the excited as well as the ground state (the frequencies do not change in the simulations reported here). They can show the vibrational dephasing rate in both electronic states and the rate of population loss due to vibrational relaxation or to nonadiabatic transfer (back electron transfer in this case). Thus these experiments will provide much more information on the excited state than is available now and will confirm or require changes to the model potential.

Fitting the difference potential to the observed optical absorption spectrum places the ground and optically excited potentials well within the Marcus inverted region. For the nearly isoenergetic states involved in natural electron transfer such placement would allow easy transfer over a low barrier. But for the optically excited state the curve crossing appears to be above the initially populated region and well above the thermally populated region. In this model the free energy curves are harmonic near equilibrium, and the equilibrium configurations in the two states differ little, except for the extension of the Cu-S(cys) bond.

Coupling of the copper center to many inhomogeneous protein modes leads to vibrations of many frequencies in the electron transfer coordinate dynamics and to vibrational relaxation on a subpicosecond time scale. The dynamics and the relaxation appear almost identical in the ground and excited states. The fast vibrational relaxation and the inaccessible curve crossing suggest that back electron transfer after excitation may initially be fast and nonthermal, but should quickly reach a slow, thermal rate. The electron transfer coordinate vibrations at specific frequencies can be partly identified using cross-correlations of the copper center internal coordinates with the difference potential. This analysis suggests that the 375 cm^{-1} vibration is mostly Cu motion against the cysteine, the 405 cm^{-1} vibration is Cu-S(cys) stretch mixed with motion of the histidine 37, and the $415\text{--}35 \text{ cm}^{-1}$ vibrations are mixed with internal vibrations of the cysteine.

Furthermore, the vibration of the Cu-S(cys) bond (and hence of the difference potential) is coupled to other nuclear coordinates in the protein. Most striking is a significant directional correlation of the motion of this bond with atomic motions throughout the protein. The vibrational couplings are formed primarily, but not exclusively, through bonded interactions, and seem particularly strong near the tyrosine 83 and histidine 87 residues through which electrons are thought to transfer in the physiological function of plastocyanin. The protein structure appears to serve dynamical functions as well as being a "rack" holding the copper center in place (Solomon et al., 1980). In general, vibrational couplings will increase fluctuations that enable forward electron transfer and speed dephasing to prevent back electron transfer. The specific vibrational correlations along

electron transfer pathways could also promote the electronic transition by, for example, directing the protein along the multidimensional potential to a region favorable to the product state. To the extent that the vibrational couplings mirror electronic couplings, plotting the correlations with the difference potential could also be a simple way of mapping out important electron transfer paths without undertaking separate calculations of all possible electronic paths.

To simulate the electronic population dynamics (the actual electron transfer) directly requires a quantum dynamical method. Indeed, the narrow electronic gap between the slightly displaced potentials should favor nuclear tunneling in the electron transfer process, thus making even semiclassical surface-hopping methods (Tully, 1990) questionable for this purpose. Furthermore, if the 20-fs excited-state lifetime estimated by Fraga et al. (1996) is correct, treatments that are perturbative in the electronic coupling will fail. Quantum simulations also will include the effects of electronic coupling on nuclear dynamics in each state: in particular, if the coupling is strong, the excited adiabatic state will have higher curvature and anharmonicity due to the avoided crossing with the ground state. The strength of the coupling and its effects can only be established by comparison of experimental studies of the rate of back electron transfer (Scherer et al., 1996) with nonadiabatic dynamics simulations.

Such quantum dynamical calculations are now in progress. The present authors are using an effective harmonic model (Cao et al., 1996) of the protein environment based on the difference potential spectral density (Fig. 4). Although the harmonic approximation appears to be justified based on the classical simulations reported here, it can obscure the information about the atomic motions that contribute to the spectral density that has been obtained using classical molecular dynamics methods in this paper. The combination of classical MD and quantum dynamical simulations with direct experimental input should therefore provide a powerful tool for the full elucidation of electron transfer dynamics.

The authors are grateful for helpful discussions and correspondence with Prof. Harry Gray, Prof. Sven Larsson, Prof. Edward Solomon, Louis LaCroix, and Lewis Book. They also thank Prof. David Christianson and Chip Lesburg for assistance with the color figure.

This research was supported by an Alfred P. Sloan Fellowship (GAV) and by a David and Lucille Packard Foundation Fellowship (NFS). NFS is an NSF National Young Investigator and an Arnold and Mabel Beckman Young Investigator.

REFERENCES

- Allen, M. P., and D. J. Tildesley. 1987. *Computer Simulation of Liquids*. Clarendon, Oxford.
- Arnett, D. C., P. Vöhringer, and N. F. Scherer. 1995. Excitation dephasing, product formation, and vibrational coherence in an intervalence charge-transfer reaction. *J. Am. Chem. Soc.* 117:12262–12272.
- Beratan, D. N., J. N. Onuchic, J. R. Winkler, and H. B. Gray. 1992. Electron-tunneling pathways in proteins. *Science*. 258:1740–1741.
- Bernhardt, P. V., and P. Comba. 1992. Molecular mechanics calculations of transition metal complexes. *Inorg. Chem.* 31:2638–2644.
- Blair, D. F., G. W. Campbell, J. R. Schoonover, S. I. Chan, H. B. Gray, B. G. Malmstrom, I. Pecht, B. I. Swanson, W. H. Woodruff, W. K. Cho, A. M. English, H. A. Fry, V. Lum, and K. A. Norton. 1985. Resonance Raman studies of blue copper proteins: effect of temperature and isotopic substitutions. Structural and thermodynamic implications. *J. Am. Chem. Soc.* 107:5755–5766.
- Brooks, B. R., R. E. Bruccoleri, B. D. Olafson, D. J. States, S. Swaminathan, and M. Karplus. 1983. CHARMM: a program for macromolecular energy, minimization, and dynamics calculations. *J. Comp. Chem.* 4:187–217.
- Brooks, C. L., M. L. Karplus, and B. M. Pettitt. 1988. Proteins: a theoretical perspective of dynamics, structure, and thermodynamics. *Adv. Chem. Phys.* Volume 71.
- Cao, J., L. W. Ungar, and G. A. Voth. 1996. A novel method for simulating quantum dissipative systems. *J. Chem. Phys.* 104:4189–4197.
- Creighton, S., J.-K. Hwang, A. Warshel, W. W. Parson, and J. Norris. 1988. Simulating the dynamics of the primary charge separation process in bacterial photosynthesis. *Biochemistry*. 27:774–781.
- Curry, W. B., M. D. Grabe, I. V. Kurnikov, S. S. Skourtis, D. N. Beratan, J. J. Regan, A. J. A. Aquino, and J. N. Onuchic. 1995. Pathways, pathway tubes, pathway docking, and propagators in electron transfer proteins. *J. Bioenerg. Biomembr.* 27:285–293.
- Dewar, M. J. S., E. G. Zoebisch, E. F. Healy, J. J. P. Stewart. 1985. A new general purpose quantum mechanical molecular model. *J. Am. Chem. Soc.* 107:3902–3909.
- Fraga, E., A. Webb, and G. R. Loppnow. 1996. Charge-transfer dynamics in plastocyanin, a blue copper protein, from resonance Raman intensities. *J. Phys. Chem.* 100:3278–3287.
- Gewirth, A. A., and E. I. Solomon. 1988. Electronic structure of plastocyanin: excited state spectral features. *J. Am. Chem. Soc.* 110:3811–3819.
- Guckert, J. A., M. D. Lowery, and E. I. Solomon. 1995. Electronic structure of the reduced blue copper active site: contributions to reduction potentials and geometry. *J. Am. Chem. Soc.* 117:2817–2844.
- Guss, J. M., H. D. Bartunik, and H. C. Freeman. 1992. Accuracy and precision in protein structure analysis: restrained least-squares refinement of the structure of poplar plastocyanin at 1.33 Å resolution. *Acta Crystallogr.* B48:790–811.
- Guss, J. M., P. R. Harrowell, M. Murata, and H. C. Freeman. 1986. Crystal structure analyses of reduced (Cu^I) poplar plastocyanin at six pH values. *J. Mol. Biol.* 192:361–387.
- He, S., S. Modi, D. S. Bendall, and J. C. Gray. 1991. The surface-exposed tyrosine residue Tyr83 of pea plastocyanin is involved in both binding and electron transfer reactions with cytochrome *f*. *EMBO J.* 10:4011–4016.
- Hoops, S. C., K. W. Anderson, and K. M. Merz, Jr. 1991. Force field design for metalloproteins. *J. Am. Chem. Soc.* 113:8262–8270.
- Hush, N. S. 1967. Intervalence-transfer absorption. Part 2. Theoretical considerations, and spectroscopic data. *Prog. Inorg. Chem.* 8:391–444.
- Jortner, J. 1976. Temperature dependent activation energy for electron transfer between biological molecules. *J. Chem. Phys.* 64:4860–4867.
- Kuki, A., and P. G. Wolynes. 1987. Electron tunneling paths in proteins. *Science*. 236:1647.
- Larsson, S., A. Broo, and L. Sjölin. 1995. Connection between structure, electronic spectrum, and electron-transfer properties of blue copper proteins. *J. Phys. Chem.* 99:4860–4865.
- Levich, V. G., and R. R. Dogonadze. 1959. Theory of nonradiation electron transitions from ion to ion solutions. *Dokl. Akad. Nauk. SSSR.* 124:123–126.
- Loppnow, G. R., and E. Fraga. 1996. Proteins as solvents: the role of amino acid composition in the excited-state charge transfer dynamics of plastocyanins. *J. Am. Chem. Soc.* submitted.
- Marchi, M., J. N. Gehlen, D. Chandler, and M. Newton. 1993. Diabatic surfaces and the pathway for primary electron transfer in a photosynthetic reaction center. *J. Am. Chem. Soc.* 115:4178–4190.

- Marcus, R. A. 1956. The theory of oxidation-reduction reactions involving electron transfer. I. *J. Chem. Phys.* 24:966-978.
- Marcus, R. A., and N. Sutin. 1985. Electron transfers in chemistry and biology. *Biochim. Biophys. Acta.* 811:265-322.
- McQuarrie, D. 1976. *Statistical Mechanics*. Harper and Row, New York.
- Merz, K. M., Jr., M. A. Murcko, and P. A. Kollman. 1991. Inhibition of carbonic anhydrase. *J. Am. Chem. Soc.* 113:4484-4490.
- Modi, S., M. Nordling, L. G. Lundberg, O. Hansson, and D. S. Bendall. 1992. Reactivity of cytochromes *c* and *f* with mutant forms of spinach plastocyanin. *Biochim. Biophys. Acta.* 1102:85-90.
- Moser, C. C., J. M. Keske, K. Warncke, R. S. Farid, and P. L. Dutton. 1992. Nature of biological electron transfer. *Nature.* 355:796-802.
- Moser, C. C., C. C. Page, R. Farid, and P. L. Dutton. 1995. Biological electron transfer. *J. Bioenerg. Biomembr.* 27:263-274.
- Myers, A. B. 1994. Relating absorption, emission, and resonance Raman spectra with electron transfer rates in photoinduced charge transfer systems: promises and pitfalls. *Chem. Phys.* 180:215-230.
- Nordling, M., K. Sigfridsson, S. Young, L. G. Lundberg, and O. Hansson. 1991. Flash-photolysis studies of the electron transfer from genetically modified spinach plastocyanin to photosystem I*. *FEBS Lett.* 291:327-330.
- Onuchic, J. N., D. N. Beratan, J. R. Winkler, and H. B. Gray. 1992. Pathway analysis of protein electron-transfer reactions. *Annu. Rev. Biophys. Biomol. Struct.* 21:349-377.
- Qiu, D., S. Dong, J. A. Ybe, M. H. Hecht, and T. G. Spiro. 1995. Variations in the type I copper protein coordination group: resonance Raman spectrum of ³⁴S-, ⁶⁵Cu-, and ¹⁵N-labeled plastocyanin. *J. Am. Chem. Soc.* 117:6443-6446.
- Qiu, D., L. Kilpatrick, N. Kitajima, and T. G. Spiro. 1994. Modeling blue copper protein resonance Raman spectra with thiolate-Cu^{II} complexes of a sterically hindered tris(pyrazolyl)borate. *J. Am. Chem. Soc.* 116:2585-2590.
- Redinbo, M. R., T. O. Yeates, and S. Merchant. 1994. Plastocyanin: structural and functional analysis. *J. Bioenerg. Biomembr.* 26:49-66.
- Reid, P. J., C. Silva, P. F. Barbara, L. Karki, and J. T. Hupp. 1995. Electronic coherence, vibrational coherence, and solvent degrees of freedom in the femtosecond spectroscopy of mixed-valence metal dimers in H₂O and D₂O. *J. Phys. Chem.* 99:2609-2616.
- Ryckaert, J. P., G. Ciccotti, and H. J. C. Berendsen. 1977. Numerical integration of the Cartesian equations of motion of a system with constraints: molecular dynamics of *n*-alkanes. *J. Comput. Phys.* 23:327.
- Scherer, N. F., L. W. Ungar, D. C. Arnett, L. D. Book, H. Hu, and G. A. Voth. 1996. Charge-transfer dynamics in blue copper proteins: experiment and simulation. In *Ultrafast Phenomena X*, Springer Series in Chemical Physics. P. F. Barbara, J. G. Fujimoto, W. H. Knox, and W. Zinth, editors. Springer-Verlag, Berlin. 361-362.
- Schulten, K., and M. Tesch. 1991. Coupling of protein motion to electron transfer: molecular dynamics, and stochastic quantum mechanics study of photosynthetic reaction centers. *Chem. Phys.* 158:421-446.
- Shen, J., and J. A. McCammon. 1991. Molecular dynamics simulation of superoxide interacting with superoxide dismutase. *Chem. Phys.* 158:191-198.
- Solomon, E. I., M. J. Baldwin, and M. D. Lowery. 1992. Electronic structures of active sites in copper proteins: contributions to reactivity. *Chem. Rev.* 92:521-542.
- Solomon, E. I., J. W. Hare, D. M. Dooley, J. H. Dawson, P. J. Stephens, and H. B. Gray. 1980. Spectroscopic studies of stellacyanin, plastocyanin, and azurin. Electronic structure of blue copper sites. *J. Am. Chem. Soc.* 102:168-178.
- Sykes, A. G. 1991a. Active-site properties of blue copper proteins. *Adv. Inorg. Chem.* 36:377-408.
- Sykes, A. G. 1991b. Plastocyanin and the blue copper proteins. *Struct. Bonding.* 75:175-224.
- Tachiya, M. 1993. Generalization of the Marcus equation for the electron-transfer rate. *J. Phys. Chem.* 97:5911-5916.
- Treutlein, H., K. Schulten, A. T. Brünger, M. Karplus, J. Deisenhofer, and H. Michel. 1992. Chromophore-protein interactions and the function of the photosynthetic reaction center: a molecular dynamics study. *Proc. Natl. Acad. Sci. USA.* 89:75-79.
- Tully, J. C. 1990. Molecular dynamics with electronic transitions. *J. Chem. Phys.* 93:1061-1071.
- Ullmann, G. M., and N. Kostić. 1995. Electron-tunneling paths in various electrostatic complexes between cytochrome *c* and plastocyanin. Anisotropy of the copper-ligand interactions, and dependence of the iron-copper electronic coupling on the metalloprotein orientation. *J. Am. Chem. Soc.* 117:4766-4774.
- Urushiyama, A., and J. Tobar. 1990. Resonance Raman active vibrations of blue copper proteins. Normal coordinate analysis on 169-atom model. *Bull. Chem. Soc. Jpn.* 63:1563-1571.
- van Gunsteren, W. F., F. J. Luque, D. Timms, and A. E. Torda. 1994. Molecular mechanics in biology: from structure to function, taking account of solvation. *Annu. Rev. Biophys. Biomol. Struct.* 23:847-863.
- Vedani, A., and D. W. Huhta. 1990. A new force field for modeling metalloproteins. *J. Am. Chem. Soc.* 112:4759-4767.
- Wampler, J. E. 1994. Computational chemistry and molecular modeling of electron-transfer proteins. *Methods Enzymol.* 243:559-607.
- Wang, C. X., A. R. Bizzarri, Y. W. Xu, and S. Cannistraro. 1994. Molecular dynamics of copper plastocyanin: simulations of structure and dynamics as a function of hydration. *Chem. Phys.* 183:155-166.
- Warshel, A., J. K. Hwang, and J. Åqvist. 1992. Computer simulations of enzymatic reactions: examination of linear free-energy relationships and quantum-mechanical corrections in the initial proton-transfer step of carbonic anhydrase. *Faraday Discuss.* 93:225-238.
- Warshel, A., and W. W. Parson. 1991. Computer simulations of electron-transfer reactions in solution and in photosynthetic reaction centers. *Annu. Rev. Phys. Chem.* 42:279-309.
- Woodruff, W. H., R. B. Dyer, and J. R. Schoonover. 1988. Resonance Raman spectroscopy of blue copper proteins. In *Biological Applications of Raman Spectroscopy*, Vol. 3. T. G. Spiro, editor. Wiley, New York. 413-438.